Available online at www.sciencedirect.com
SCIENCE DIRECT®
Carbohydrate Research 339 (2004) 1697–1709
Carbohydrate RESEARCH

Effect of methylation on the stability and solvation free energy of amylose and cellulose fragments: a molecular dynamics study

Haibo Yu,[a] Manfred Amann,[b] Tomas Hansson,[a,†] Jutta Köhler,[b] Günter Wich[b] and Wilfred F. van Gunsteren[a,*]

[a]*Laboratory of Physical Chemistry, Swiss Federal Institute of Technology Zürich, ETH Hönggerberg, 8093 Zürich, Switzerland*
[b]*Wacker-Chemie, Consortium für Elektrochemische Industrie GmbH, Zielstattstr 20, D-81379 Munich, Germany*

Received 8 November 2003; revised 6 March 2004; accepted 3 May 2004

Abstract—Molecular dynamics (MD) simulations were used to study the stability and solvation of amylose and cellulose fragments. The recently developed GROMOS carbohydrate force field was further tested by simulating maltose, cellobiose, and maltoheptaose. The MD simulations reproduced fairly well the favorable conformations of disaccharides defined by the torsional angles related with the glycosidic bond and the radius gyration of maltoheptaose. The effects of methylation at different hydroxyl groups on the stability of amylose and cellulose fragments were investigated. The methylations of O-2 and O-3 reduce the stability of a single helix more than methylation at O-6, while the latter reduces the stability of a double helix more. Solvation free-energy differences between the unsubstituted amylose and cellulose fragments and the methylated species were studied using the single-step perturbation method. It was found that methylation at O-2 has the biggest effect, in agreement with experiment.

Keywords: Computer simulation; Molecular dynamics; Amylose; Cellulose; Stability; Free energy; Single-step perturbation

1. Introduction

Starch and cellulose are abundant natural biomolecules connected with glucose. Both of these compounds have 1,4-linked bonds between glucopyranosyl units and they differ only in their anomeric configuration. Starch contains two kinds of polysaccharides: amylose and amylopectin. Amylose, defined as a linear molecule of α-(1→4)-D-glucopyranosyl units, occurs in three allomorphs, known as the A, B, and V forms.[1] The A and B forms both consist of left-handed double helices with six glucopyranosyl units per turn and appear to differ only in the packing of the starch helices: the A form crystallizes in a monoclinic unit cell (space group $B2$)[2] and the B form in a hexagonal unit cell (space group $P6_1$).[3] V-Amylose is a generic term for amylose obtained as single helices cocrystallized with compounds such as iodine, DMSO, alcohols, or fatty acids. Although such compounds are required for formation of the V-type form, they are not systematically included in the amylose helix.[4,5] Saitô et al.[6] found that the helical conformations ascribed to both V- and B-types are not very different. Cellulose is a linear polymer of β-(1→4)-D-glucopyranosyl units and is the most abundant natural polymer on earth. Despite the considerable degree to which cellulose has been investigated, its detailed crystal structure has not been identified with absolute clarity and is still a matter of debate.[7,8] Though ambiguity exists regarding the detailed atomic structure of cellulose, experiments such as X-ray scattering and electron diffraction show that cellulose aggregates in a fully extended conformation to form a sheet-like structure.

The geometry of the α (axial) and β (equatorial) bonds from carbon 1 endows amylose and cellulose with

* Corresponding author. Tel.: +41-1-632 5502; fax: +41-1-632 1039; e-mail addresses: wfvgn@igc.phys.chem.ethz.ch; igc-sec@igc.phys.chem.ethz.ch
† Present address: Karo Bio AB, Novum, S-141 57 Huddinge, Sweden.

0008-6215/$ - see front matter © 2004 Elsevier Ltd. All rights reserved.
doi:10.1016/j.carres.2004.05.003

Table 1. Overview of the MD simulations of the different systems

Simulation label	Solute			Number of water molecules	Simulation length (ns)
	Polysaccharides	Number of glucopyranosyl units	Initial conformation		
Maltose	Maltose	2	Extended	968	2
Cellobiose	Cellobiose	2	Extended	1053	2
SH7	Maltoheptaose	7	L-helix	5324	5
SH, SH6Me, SH23Me, SH236Me, SHPERT	Maltononaose or methylated derivatives	9	L-helix	7978	5
SE, SEPERT	Maltononaose	9	Extended	8364	5
DP, DP6Me, DP23Me, DP236Me	Maltononaose or methylated derivatives	2×9	Double L-helix	7990	5
CE, CE6Me, CE23Me, CE236Me, CEPERT	Cellononaose or methylated derivatives	9	Extended	11,176	5

The systems are: maltose (α-D-glucopyranosyl-(1→4)-α-D-glucopyranose), cellobiose (β-D-glucopyranosyl-(1→4)-β-D-glucopyranose), SH7 (maltoheptaose, starting from a left-handed helical structure), SH (maltononaose, starting from a left-handed helical structure), SH6Me (as SH, but with glucopyranosyl units 2, 4, 6, and 8 methylated at O-6), SH23Me (as SH, but with glucopyranosyl units 2 and 6 methylated at O-2 and glucopyranosyl units 4 and 8 methylated at O-3), SH236Me (as SH, but with glucopyranosyl units 1, 3, 5, 7, and 9 methylated at O-6, glucopyranosyl units 2 and 6 methylated at O-2 and glucopyranosyl units 4 and 8 methylated at O-3), SHPERT (as SH, but with soft-core atoms at H-2, H-3, and H-6 of all glucopyranosyl units, see Section 4 for details), SE (maltononaose, starting from an extended conformation), SEPERT (as SE, but with soft-core atoms at H-2, H-3, and H-6 of all glucopyranosyl units, see Section 4 for details), DP (two maltononaoses, starting from a parallel double left-handed helix), DP6Me (as DP, but with methylations as indicated by 6Me), DP23Me (as DP, but with methylations as indicated by 23Me), DP236Me (as DP, but with methylations as indicated by 236Me), CE (cellononaose, starting from an extended structure), CE6Me (as CE, but with methylations as indicated by 6Me), CE23Me (as CE, but with methylations as indicated by 23Me), CE236Me (as CE, but with methylations as indicated by 236Me), CEPERT (as CE, but with soft-core atoms at H-2, H-3, and H-6 of all glucopyranosyl units, see Section 4 for details).

very different physical and biological properties.[9] Amylose is poorly soluble in water but forms suspensions, in which it is helical. While the special structure of cellulose gives cellulose fibers exceptional strength and makes them insoluble in water despite their hydrophilicity, extensive pores inside cellulose fibers can hold a large amount of water. Cellulose has a close relation to human life functioning as paper, textile, and building material.

Due to the biological availability and commercial importance of cellulose, for many years much effort has been spent to improve the technical properties of cellulose in order to add new functions to it, for example, by the investigation of cellulose derivatives. On the other hand, since starch is the most abundant biomolecule on earth after cellulose and readily available and since it differs from cellulose only in anomeric configuration, one might think of producing starch (amylose) derivatives that have more cellulose-like structure, properties, and functions. For example, at which sites should starch be methylated to bestow it with cellulose-like properties? Methylation of particular hydroxyl groups will change the hydrogen-bonding capacity, and may thus change the properties of amylose and cellulose: their preferred conformations and their solvation free energy.

Molecular dynamics (MD) simulation studies of carbohydrates in the literature[10,11] deal with maltose or cellobiose composed of two glucose units[12–16] or with cyclic chains including α-, β, and γ-cyclodextrins[17–23] as well as the single glucose units of α- and β-anomers.[15,24,25] However, there are only a few studies dealing with longer amylose or cellulose chains.[26,27] It is the purpose of our work to study the properties of longer amylose and cellulose chains in atomic detail using 19 MD simulations (Table 1) including an explicit representation of solvent molecules, in order to address the following three aspects of polysaccharide behaviors:

1. The ability of the interatomic force field used to adequately mimic the conformational behavior of sugar molecules is tested by a comparison of experimental data (ϕ, ψ-torsional angles, C–H vector order parameters, and radius of gyration), derived from nuclear magnetic resonance (NMR) spectroscopy and X-ray crystallography, available for the shorter polysaccharides maltose, cellobiose, and maltoheptaose (SH7), to simulated values for these quantities.
2. A glucopyranosyl unit can be methylated at three sites, O-2, O-3, and O-6, in order to change the conformational behaviors of polysaccharides. We chose to study polysaccharides consisting of nine glucopyranosyl units, which are sufficiently long to be able to form helical structures and sufficiently short to allow for simulation. In a nonamer, there are 27 possible methylation sites, which means there exist $2^{27} - 1 = 134,217,727$ methylated derivatives of a nonaose. We chose three methylation patterns (denoted by the suffixes 6Me, 23Me, and 236Me indicating methylation at different hydroxyl sites) for investigation by separate MD simulations for three different systems: single strand maltononaose starting from helical (SH) or extended (SE) structures, double strand helical maltononaose (DP), and single strand cellononaose (CE), resulting in 13 separate simula-

tions, for which the conformational properties are studied.

3. An alternative way to study the stability of a particular distribution of conformers is to apply the single-step perturbation technique[28] to obtain from one simulation (indicated by SHPERT, SEPERT, and CEPERT for the three systems mentioned above) the difference in free energy of solvation between a great many methylated derivatives and the 'native' polysaccharides. Although we could calculate all 134,217,727 free-energy differences for all methylated derivatives, we only reported 31 of these. These concern relatively simple methylation patterns, which may give an indication of the effects of a particular methylation on the stability of the molecule.

2. Results

2.1. Force-field testing

Molecular dynamics simulations were performed on maltose, cellobiose, and maltoheptaose (see Table 1) in water to validate the recently developed GROMOS carbohydrate force field. From experimental NMR studies the favorable conformations for maltose in aqueous solution, as defined by two dihedral angles (ϕ, ψ) ($\phi = \angle$O-5–C-1–O-4′–C-4′ and $\psi = \angle$C-1–O-4′–C-4′–C-5′), could be derived: (75°, −170°),[29] (91°, −147°)[30] (Pérez et al.[30] observed four favorable conformations: 18% (110°, −115°), 26% (100°, −135°), 26% (80°, −150°), and 30% (90°, 80°)), (84°, −140°)[31] (Shashkov et al.[31] observed four favorable conformations: 40% (50°, −160°), 45% (90°, −140°), 12% (140°, −100°), and 3% (90°, 80°)), and (88°, −144°).[32] In addition, optical rotation dispersion (ORD) experiments[33] have indicated two favorable conformations at (50°, −160°) and (90°, −135°). The (ϕ, ψ) distributions from the 2 ns MD simulations are shown in Figure 1 together with the ideal values derived from NMR and ORD. The same comparison was done for cellobiose and the results are shown in Figure 2 together with the experimental data obtained from a crystal structure (−78°, −138°)[12] and from NMR (−75°, −158°),[12] (−88°, −141°).[32] In the NMR studies the torsional angle values were derived from ^3J-coupling constants using a Karplus-type equation,[34,35] which procedure does introduce uncertainty.[29–32,12,36] In X-ray crystallographic studies, one usually observes one single conformation, which may not be representative for the ensemble of conformations present in solution.[37] The MD simulations show a distribution of (ϕ, ψ) torsional angle values in which the values derived from NMR and X-ray experiments are contained. The orientations of the glycosidic bonds in the disaccharides are on average reproduced.

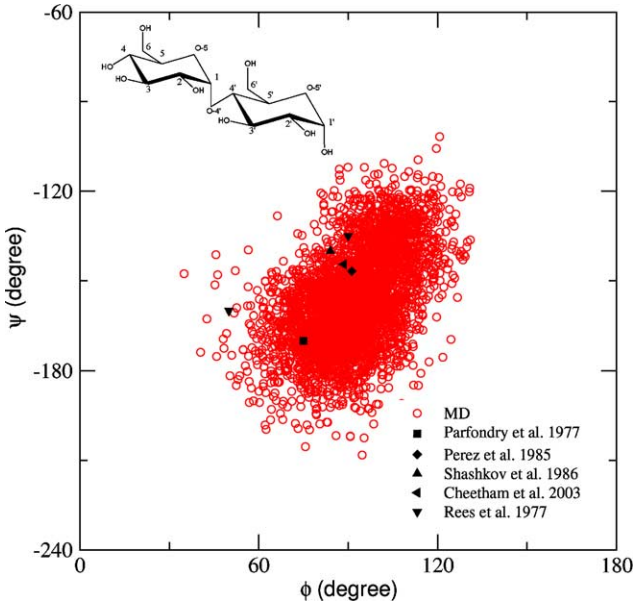

Figure 1. The distribution of ϕ and ψ torsional angles of maltose from MD simulation (2 ns) in water. ϕ and ψ are defined by the atoms O-5–C-1–O-4′–C-4′ and C-1–O-4′–C-1′–C-5′, respectively. The experimental values derived from NMR and ORD studies were taken from Refs. 29–33.

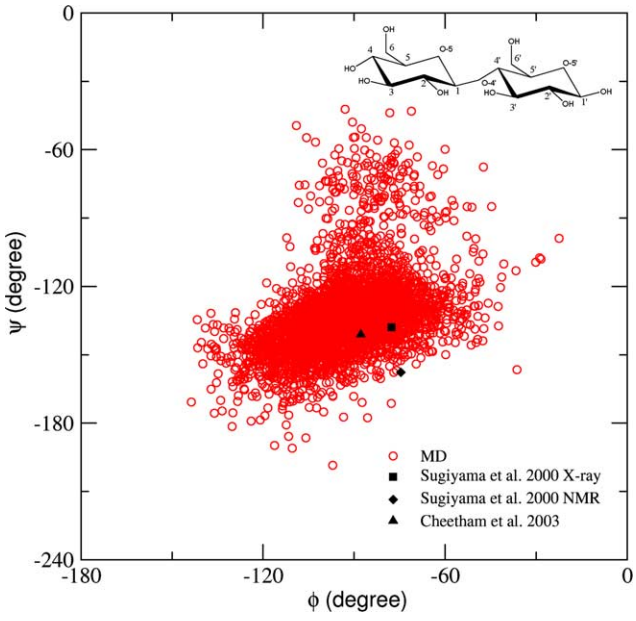

Figure 2. The distribution of ϕ and ψ torsional angles of cellobiose from MD simulation (2 ns) in water. ϕ and ψ are defined by the atoms O-5–C-1–O-4′–C-4′ and C-1–O-4′–C-1′–C-5′, respectively. The experimental values derived from X-ray and NMR studies were taken from Refs. 12 and 32.

Order parameters of the C–H bond vectors in maltose were calculated using Eq. 5 (see Section 4) and compared with the values derived from experimental relaxation parameters.[13] As can be seen from Figure 3, the values for the C–H vectors in the six-membered rings are

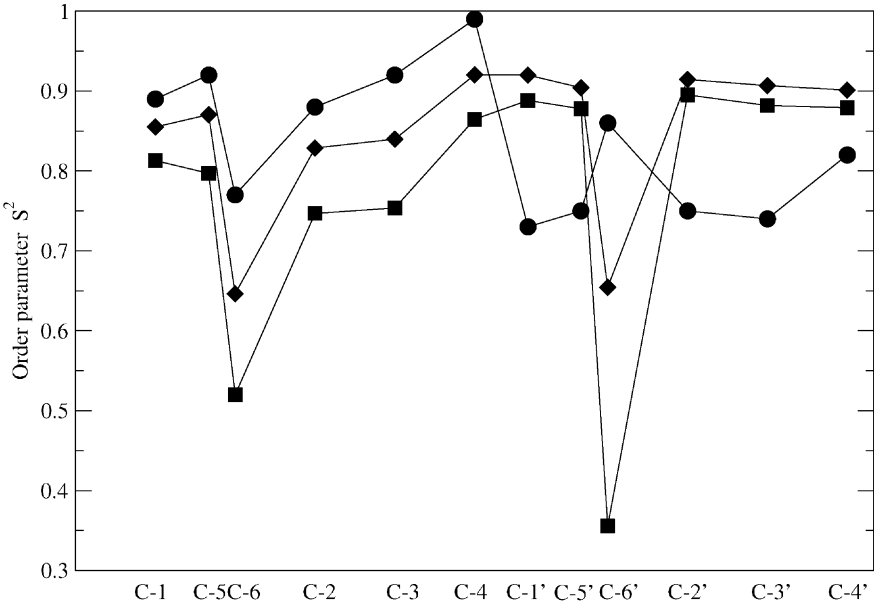

Figure 3. Order parameters S^2 for C–H vectors in maltose calculated from simulation (2 ns) and from experimental relaxation parameters (circles).[13] For the atom names, see Figure 1. The order parameters were defined according to Eqs. 3 and 4 (see Section 4 for more details). The S^2 order parameters were calculated using Eq. 5 in two different ways using the configurations from the 2 ns simulation at 0.5 ps intervals: either by averaging over the whole simulation period (squares) or by using a 25 ps averaging window (diamonds) that is moved through the whole 2 ns analysis period.[39]

relatively large indicating that maltose and its six-membered glycosyl unit are quite rigid. Due to greater freedom of motion, in the simulation the C-6–H-6 and C-6′–H-6′ vectors have much lower order parameters than those within the ring, while in the experiment the C-6–H-6 and C-6′–H-6′ vectors have order parameters comparable to those within the ring. As pointed out in Ref. 13, the large order parameter for the C-6′–H-6′ vector as derived from experiments is probably due to the approximation of treating the translational and rotational motions separately in the so-called model-free approach to derive the order parameters from experimental data.[38–40] In the maltoheptaose simulation, the averages of (ϕ, ψ) are (92°, −148°), which is comparable to the values derived from an NMR study of maltoheptaose (87°, −141°).[41]

The radius of gyration (R_{gyr}) of maltoheptaose was calculated from the simulation starting from the helical structure. Figure 4 shows R_{gyr} plotted against time and the horizontal dashed lines represent the range of experimental values derived from small-angle X-ray scattering.[27] The average value of 0.90 nm for R_{gyr} is higher than the experimental one of 0.74 ± 0.02 nm.[27] However, using the regular amylose helical structure,[3] R_{gyr} is about 0.83 nm, which value is also larger than the one derived from small-angle X-ray scattering. Moreover, the simulated values for R_{gyr} fluctuate in the range 0.73–1.02 nm.

Overall the simulations described yield results, which are in agreement with experimental data, thus validating the use of the new GROMOS carbohydrate force field in the following studies.

2.2. Stability and conformation of amylose and cellulose fragments

2.2.1. Amylose fragments containing nine glucopyranosyl units. The MD of single helical maltononaose and methylated derivatives thereof was simulated, each for 5 ns. The atom-positional root-mean-square deviations (RMSD) with respect to the model (single-helical) structure of maltononaose in the simulations SH, SE, SH6Me, SH23Me, and SH236Me (see Table 1) as a function of simulation time are shown in Figure 5, Panel A. Compared to SH6Me, the methylation at O-2 and O-3 has the larger effects on the stability of helical structure, while the distributions of ϕ and ψ for SH, SH6Me, SH23Me, and SH236Me show little differences as shown in Figure 6 Panel A. The averages of ϕ and ψ in the simulations SH, SH6Me, SH23Me, and SH236Me are (84°, −148°), (85°, −147°), (82°, −147°), and (82°, −149°), respectively, which are comparable to the parameters proposed for the regular helix: (84°, −145°) by Imberty and Pérez[3] and (82°, −132°) for short-chain amylose inferred from NMR by Sugiyama et al.[41] Starting from the extended form, simulation SE converged to the helical-like structure within 5 ns simulation with similar distributions for the angles ϕ and ψ. The central member of the second most populated cluster of trajectory structures of simulation SE (population 10%) has an RMSD of only 0.18 nm to the central member of the first, most populated (helical) cluster of trajectory structures of simulation SH. The occurrences (in %) of the 'native' hydrogen bonds formed by O-3–H-3 of one glucopyranosyl unit to the O-2 of the adjacent gluco-

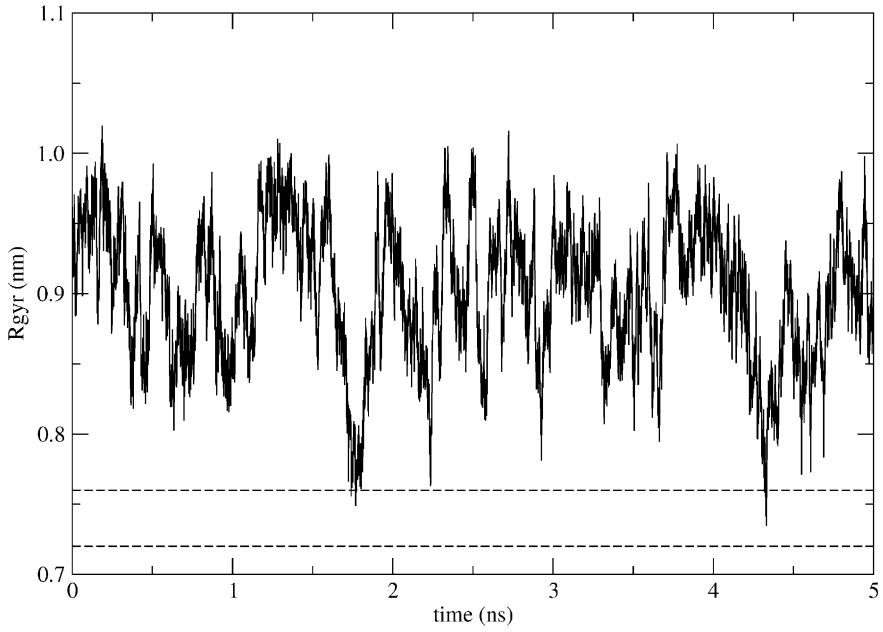

Figure 4. Radius of gyration (R_{gyr}) of maltoheptaose plotted against simulation time. The horizontal dashed lines represent the value of 0.74 ± 0.02 nm derived from experiment.[27]

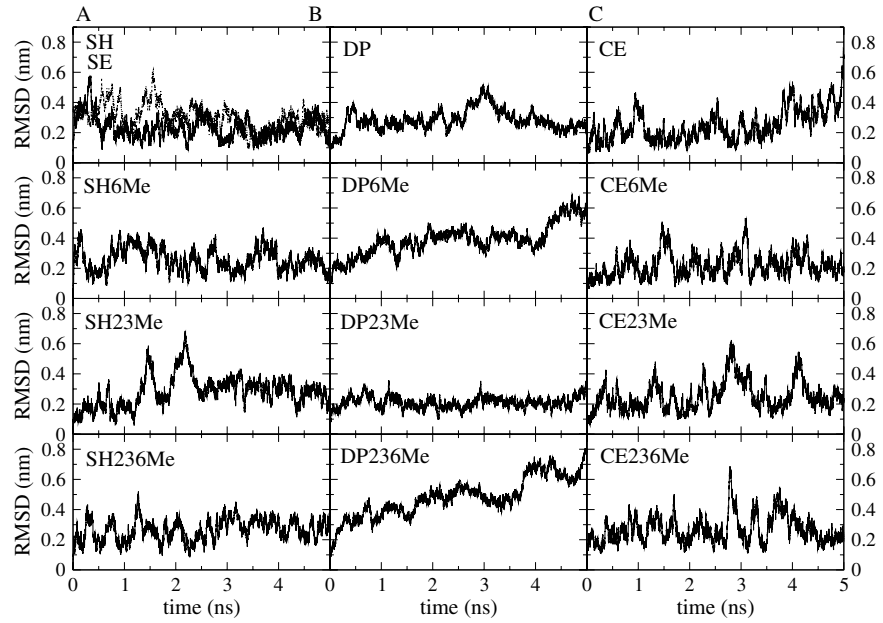

Figure 5. The atom-positional root-mean-square deviations (RMSD) of the atoms O-1, C-1, C-2, C-3, C-4, C-5, and O-5 with respect to the starting (helical) structure as a function of time for the simulations SH (solid line)/SE (dotted line), SH6Me, SH23Me, SH236Me (Panel A), DP, DP6Me, DP23Me, DP236Me (Panel B), CE, CE6Me, CE23Me, and CE236Me (Panel C). For further information see Table 1.

pyranosyl unit in various simulations are listed in Table 2. Methylation at O-3 removes the possibility for a single helix to form intrastrand hydrogen bonds, thus affecting the stability. Conformational cluster analyses show that the trajectories of the simulations SH, SH6Me, SH23Me, and SH236Me yield 20 clusters out of 79, 20 clusters out of 77, 22 clusters out of 88, and 21 clusters out of 76 in total, respectively, that have a population larger than 1%. The central members of the first, most populated, clusters of simulations SH, SH6Me, SH23Me, and SH236Me are shown in Figure 7A–D. Conformational cluster analyses using a criterion of an RMSD of 0.15 nm on the merged trajectories of pairs of simulations (Fig. 8, Panel A) show that

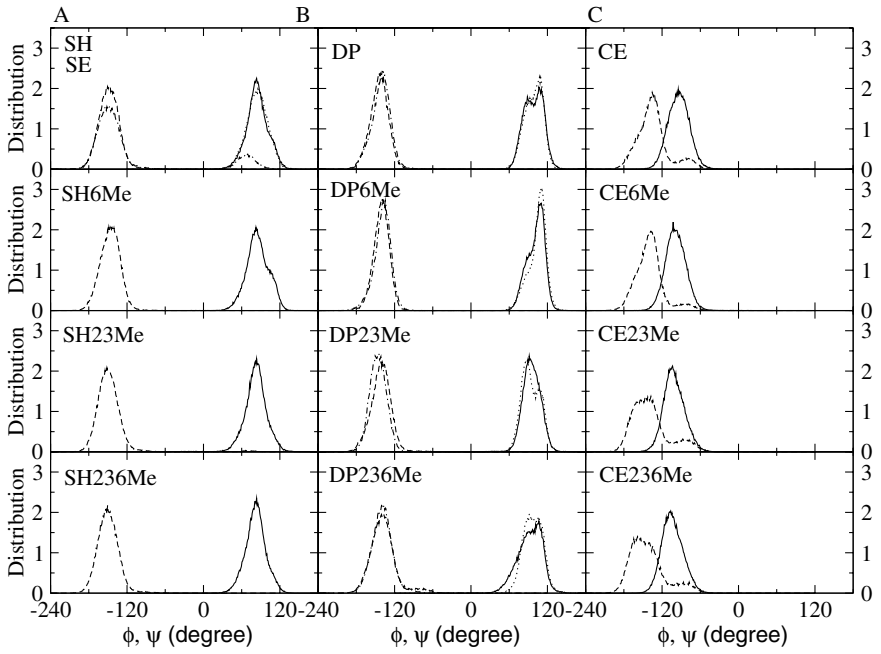

Figure 6. The distribution (arbitrary units) of the torsional angles ϕ(∠O-5–C-1–O-4′–C-4′) (solid or dotted line) and ψ(∠C-1–O-4′–C-1′–C-5′) (dashed or dot-dashed line) for SH (solid and dashed)/SE (dotted and dot-dashed), SH6Me, SH23Me, SH236Me (Panel A, solid line: ϕ, dashed line: ψ), DP, DP6Me, DP23Me, DP236Me (Panel B, solid line and dotted line: ϕ, dashed line and dot-dashed line: ψ), CE, CE6Me, CE23Me, and CE236Me (Panel C, solid line: ϕ, dashed line: ψ).

simulation SH shares more conformational space with simulation SH6Me than with simulations SH23Me and SH236Me.

The MD of a double helical pair of maltononaose molecules and its methylated derivatives was simulated, each for 5 ns. Contrary to single helix systems, methylation at O-6 affects the stability of the double helix more than at O-2 or O-3 (Fig. 5, Panel B). The methylated derivative DP23Me shows somewhat stronger hydrogen bonding between the two molecules than the unsubstituted DP, which may be due to the fact that methylation at O-2 and O-3 removes the possibility of forming 'nonnative' interstrand hydrogen bonds and thus stabilizes the 'native' interstrand hydrogen bonds (Table 2). As for the distribution of the angles ϕ and ψ, simulation DP6Me favors a slightly larger ϕ while simulation DP23Me favors a slightly smaller ψ (Fig. 6, Panel B). Conformational cluster analyses show that simulations DP, DP6Me, DP23Me, and DP236Me yield 5 clusters out of 16, 12 clusters out of 25, 4 clusters out of 8, and 11 clusters out of 26 in total, respectively, that have a population larger than 1%. The central members of the first, most populated, clusters of simulations DP, DP6Me, DP23Me, and DP236Me are shown in Figure 7E–H. Using a cluster criterion of an RMSD of 0.21 nm, simulation DP shows little overlap in conformational space with simulations DP6Me, DP23Me, and DP236Me, while the first chain of the double helix in simulation DP does show some overlap with simulation SH using a criterion of an RMSD of 0.15 nm (Fig. 8, Panel B). Although the helical conformation in simulation DP23Me is very stable during the 5 ns simulation with an RMSD with respect to the initial double helical structure around 0.20 nm (Fig. 5, Panel B), the conformational spaces sampled in simulations DP and DP23Me are quite different (Fig. 8, Panel B).

In conclusion, the simulations of single helical amylose fragments and methylation derivatives point to a retaining of overall helical structure, irrespective of methylation, but with larger fluctuations around the average structure in the O-2-, O-3-methylated case, while the simulations of double helical pairs of amylose fragments and their corresponding methylated derivatives show a stabilization of the double helix upon O-2-, O-3-methylation and a destabilization by O-6-methylation.

2.2.2. Cellulose fragments containing nine glucopyranosyl units. The MD of an extended cellononaose molecule and methylated derivatives thereof was simulated, each for 5 ns. In the simulation CE of cellononaose, the atom-positional RMSD with respect to the extended starting conformation (Fig. 5 Panel C) increases to about 0.6 nm. Analyzing the trajectory structures we found that this corresponds to a bending of the molecule. Extending the simulation beyond 5 ns, the molecule adopted again extended conformations (data not shown). The averages of the angles (ϕ, ψ) in simulations CE, CE6Me, CE23Me, and CE236Me are (−94°, −134°), (−99°, −139°), (−101°, −139°), and (−104°, −143°),

Table 2. Occurrences of hydrogen bonds (in %) during the 5 ns simulations

	SH	SH6Me	SH23Me	SH236Me	DP		DP6Me		DP23Me		DP236Me		CE	CE6Me	CE23Me	CE236Me
8O3H3–9O2	20	6			23	17	44	52								
7O3H3–8O2	10	10	4	4	26	1	40	55	0	24	18	60				
6O3H3–7O2	10	2	15	21	27	1	34	31	23	47	21	25				
5O3H3–6O2	20	3	1	1	31	36	27	58	7	2	3	22				
4O3H3–5O2	19	28			26	68	52	56								
3O3H3–4O2	0	21	8	8	91	81	73	62	46	51	58	51				
2O3H3–3O2	0	21	16	15	58	73	74	87	54	72	57	48				
1O3H3–2O2	9	30	7	5	3	49	68	80	22	19	37	2				
8O3H3–9O5													11	19		
7O3H3–8O5													65	40	53	3
6O3H3–7O5													53	46	5	42
5O3H3–6O5													49	28	41	25
4O3H3–5O5													54	60		
3O3H3–4O5													60	71	26	15
2O3H3–3O5													54	23	34	24
1O3H3–2O5													4	70	3	29
7O6H6–9′O2					0	7	0	0	4	6						
6O6H6–8′O2					9	2			11	29	6	0				
5O6H6–7′O2					46	7	15	12	21	26						
4O6H6–6′O2					3	39			30	24	0	0				
3O6H6–5′O2					3	4	4	3	4	20						
2O6H6–4′O2					3	5			8	18	3	0				
1O6H6–3′O2					3	8	1	2	2	5						
9O2H2–7′O6					0	7	1	0	37	8	1	0				
8O2H2–6′O6					4	37	0	1	30	1	0	0				
7O2H2–5′O6					0	23	6	0	19	5	0	0				
6O2H2–4′O6					1	25	0	0								
5O2H2–3′O6					34	0	4	0	12	31	0	0				
4O2H2–2′O6					10	2	0	1	5	30	6	26				
3O2H2–1′O6					3	3	9	6	4	2	0	0				

A hydrogen bond is assumed to exist if the hydrogen–acceptor distance is smaller than 0.25 nm and the donor–hydrogen–acceptor angle is larger than 135°. For further information, see caption Table 1.

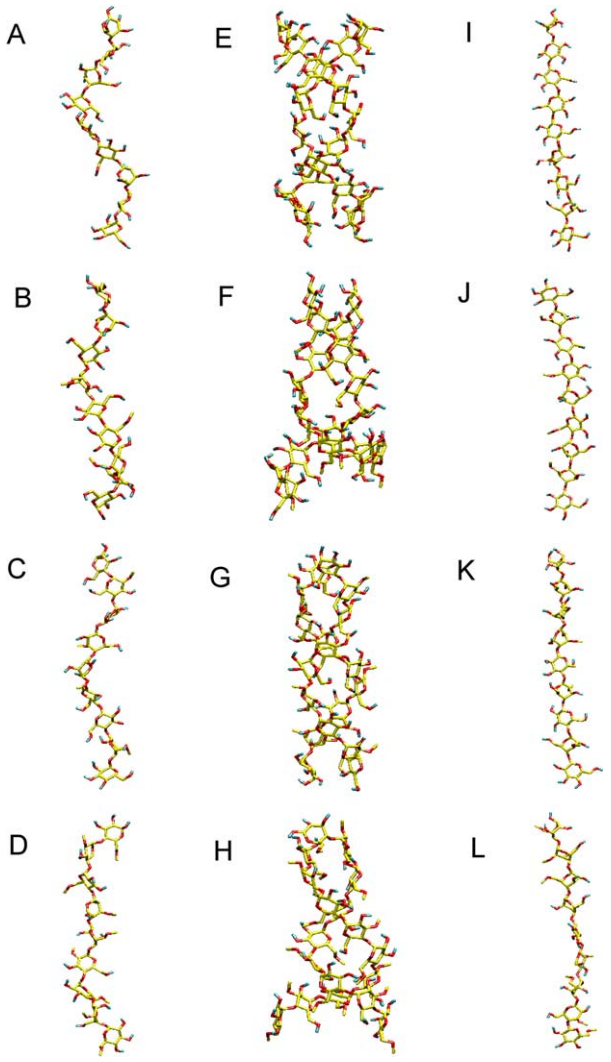

Figure 7. Conformation of the central members of the first, most populated, clusters in the simulations SH (A, population 17%, structure at 3.72 ns), SH6Me (B, population 16%, structure at 2.49 ns), SH23Me (C, population 15%, structure at 2.75 ns), SH236Me (D, population 22%, structure at 4.34 ns), DP (E, population 46%, structure at 2.34 ns), DP6Me (F, population 42%, structure at 3.81 ns), DP23Me (G, population 89%, structure at 2.56 ns), DP236Me (H, population 24%, structure at 0.55 ns), CE (I, population 20%, structure at 2.79 ns), CE6Me (J, population 20%, structure at 3.96 ns), CE23Me (K, population 14%, structure at 3.61 ns), and CE236Me (L, population 10%, structure at 4.78 ns). The conformational cluster analyses were performed based on the root-mean-square deviations (RMSD) of atoms C-1, C-2, C-3, C-4, O-4, C-5, and O-5 with a criterion of 0.15 nm for SH, SH6Me, SH23Me, SH236Me, CE, CE6Me, CE23Me, and CE236Me and of 0.21 nm for DP, DP6Me, DP23Me, and DP236Me.

respectively. They are very close to the values derived from experiments.[8] Regarding the distribution of the ϕ and ψ angles, there exist differences between the simulations CE, CE6Me, CE23Me, and CE236Me, as shown in Figure 6, Panel C. Methylation at O-2 and O-3 favors a broader distribution of ψ. The methylation at O-3 removes the hydrogen bonding capacity between O-3–H-3 and the adjacent O5 atom (Table 2). For cellulose fragments, the methylation has less effect on the stability of 'native' hydrogen bonds compared to amylose fragments, as shown in Table 2. Conformational cluster analyses show that the trajectories of simulations CE, CE6Me, CE23Me, and CE236Me yield 19 clusters out of 67, 21 clusters out of 67, 23 clusters out of 84, and 27 clusters out of 89 in total, respectively, that have a population larger than 1%. As shown in Figure 7I–L, the central members of the first, most populated, clusters in the four simulations are extended conformations. By cluster analysis on the merged trajectories of pairs of simulations, we found that simulation CE does share considerably conformational space with simulations CE6Me, CE23Me, and CE236Me (Fig. 8, Panel C).

Taken together, the simulations of cellononaose and methylated derivatives show that the extended conformation of the nonamer is not significantly changed by methylation.

2.3. Solvation free-energy differences

MD was simulated for 5 ns of amylose-like nonamers (maltononaose), starting from both extended and single helical (simulations SEPERT and SHPERT) conformations, and of cellulose-like nonamer (cellononaose, simulation CEPERT) starting from an extended conformation. In all three cases, the hydrogens of all C-2, C-3, and C-6 hydroxyl groups were treated as 'soft methylated' that is, bearing soft-core Lennard–Jones and electrostatic potentials. These simulations were performed to estimate the solvation free-energy differences between the amylose and the cellulose fragments and a variety of their methylated derivatives using the single-step perturbation method (see Eq. 2, Section 4). The computed estimates are shown in Table 3.

Comparing the values calculated from the 5 ns simulations and those from the last 2 ns of the simulations, the solvation free-energy differences between CE and its methylated derivatives converged within 5 ns of simulation, especially for the single mutation at O-2 the root-mean-square difference is about 1.4 kJ mol^{-1}, while those for both the SH and SE simulations did not converge within 5 ns of simulation. The fast convergence displayed by the cellulose system is due to the stiffness of cellulose fragments, which means that less conformations must be sampled.

Comparing a single methylation at O-2, O-3, or O-6, the solvation free-energy difference $\Delta\Delta G$ caused by methylation at O-2 is the biggest with an average over the full 5 ns (last 2 ns) of 40 (36), 49 (31), and 43 (42) kJ mol^{-1} in the simulations of SH(SHPERT), SE(SEPERT), and CE(CEPERT), respectively. This has been observed in experiments (personal communication, Manfred Amann).

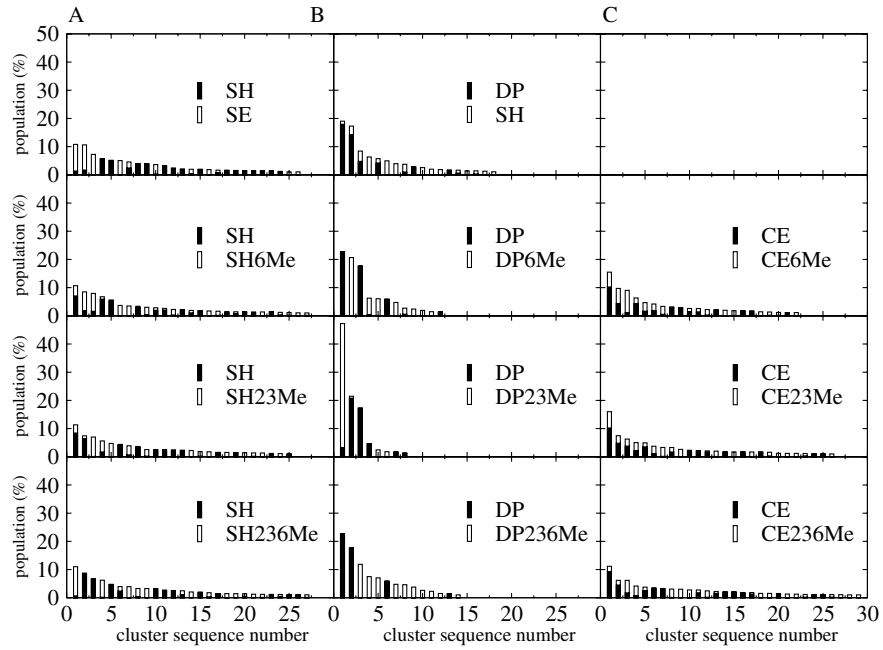

Figure 8. Population of clusters (more than 1% population) determined for merged trajectories of pairs of simulations, which include 10,000 structures (at 1 ps intervals) from the two simulations. As for the comparison between DP and SH, only the first chain of the double helix in DP is considered.

Table 3. Solvation free-energy differences (in kJ mol^{-1}) of methylation at different hydroxyl groups with respect to the unsubstituted SH, SE, and CE molecules

Site	SHPERT			SEPERT			CEPERT		
	2	3	6	2	3	6	2	3	6
$\Delta\Delta G_{1OH}$	54 (37)	28 (6)	−1 (17)	68 (18)	9 (−2)	26 (−11)	53 (53)	18 (27)	10 (10)
$\Delta\Delta G_{2OH}$	46 (27)	−32 (7)	15 (35)	54 (32)	28 (38)	9 (1)	48 (48)	12 (11)	32 (32)
$\Delta\Delta G_{3OH}$	31 (35)	−30 (22)	7 (16)	57 (23)	5 (11)	21 (8)	28 (28)	18 (14)	21 (12)
$\Delta\Delta G_{4OH}$	64 (34)	−17 (19)	−6 (10)	50 (37)	29 (41)	14 (20)	34 (32)	30 (30)	0 (−4)
$\Delta\Delta G_{5OH}$	17 (34)	3 (12)	−2 (15)	47 (58)	44 (15)	34 (13)	27 (27)	25 (25)	18 (10)
$\Delta\Delta G_{6OH}$	19 (42)	−24 (6)	16 (34)	40 (19)	24 (0)	21 (18)	43 (42)	36 (36)	17 (15)
$\Delta\Delta G_{7OH}$	40 (37)	10 (16)	6 (24)	48 (17)	7 (6)	18 (8)	60 (60)	34 (11)	16 (10)
$\Delta\Delta G_{8OH}$	35 (30)	−5 (29)	26 (9)	46 (33)	43 (4)	30 (−8)	65 (65)	17 (11)	15 (14)
$\Delta\Delta G_{9OH}$	53 (52)	0 (33)	14 (23)	34 (39)	41 (30)	22 (−17)	30 (27)	27 (27)	27 (27)
$\Delta\Delta G_{mean}$	40 (36)	−7 (17)	8 (20)	49 (31)	26 (16)	22 (4)	43 (42)	24 (21)	17 (14)
$\Delta\Delta G_{6Me}$			45 (86)			58 (42)			68 (50)
$\Delta\Delta G_{23Me}$	93 (121)			128 (90)			136 (136)		
$\Delta\Delta G_{236Me}$		157 (184)			247 (170)			224 (165)	
$\Delta\Delta G_{all}$		365 (432)			367 (368)			393 (329)	

The free-energy calculations were done for the entire 5 ns simulations as well as for the last 2 ns parts of the simulations (listed between parentheses). $\Delta\Delta G_{nOH}$ represents the solvation free-energy difference between the methylated derivative with a single methylation at O-2, O-3, or O-6 on the nth glucopyranosyl unit and the unsubstituted SH (SE or CE) molecule, while $\Delta\Delta G_{mean}$ denotes the corresponding averages over the nine glucopyranosyl units. $\Delta\Delta G_{6Me}$ represents the solvation free-energy difference between the SH6Me and SH molecules, between the SE6Me and SE molecules, and between the CE6Me and CE molecules (four sites). $\Delta\Delta G_{23Me}$ represents the solvation free-energy difference between the SH23Me and SH molecules, between the SE23Me and SE molecules, and between the CE23Me and CE molecules (four sites). $\Delta\Delta G_{236Me}$ represents the solvation free-energy difference between the SH236Me and SH molecules, between the SE236Me and SE molecules, and between the CE236Me and CE molecules (nine sites). $\Delta\Delta G_{all}$ represents the solvation free-energy difference between the methylated derivatives with all (27) possible methylations (except at the two-terminal hydroxyl groups) and the SH, SE, and CE molecules.

Considering multiple-site methylations (e.g., $\Delta\Delta G_{6Me}$, $\Delta\Delta G_{23Me}$, and $\Delta\Delta G_{236Me}$) in Table 3, the free-energy differences of the single-site ones are approximately additive provided that the different methylation sites are far away from each other. For those methylation sites that are close to each other, the free-energy differences are cooperative that is the free-energy difference for a double methylation is not close to the sum of the two free-energy differences for the corresponding single methylations.

The free-energy differences caused by methylations in amylose in extended form (SE) are very similar to those in cellulose in extended form (CE), whereas larger differences are observed between the free-energy differences of amylose in helical (SH) versus extended (SE) form. This suggests that forcing amylose to a cellulose-like (extended) structure will make amylose derivatives adopt the properties of cellulose.

3. Conclusions

In the present work, MD simulations including explicitly modeled water molecules were performed to study the conformation and solvation of maltononaose and cellononaose and a number of methylated derivatives.

In the simulations of amylose fragments, methylation at O-2 and O-3 affects the stability of a single helix more than that at O-6, while the stability of a double helix of amylose fragments is most reduced by methylation at O-6. Methylation has less effect on the stability of cellulose fragments. Generally, the methylations do not induce dramatical structural changes in the most stable conformations of amylose and cellulose fragments. With respect to the solvation free-energy differences, methylation at O-2 has the biggest effect on both amylose and cellulose fragments, which is in line with experimental data. The simulation results suggest that in order to produce amylose derivatives with cellulose-like properties (both structural and solvational) from amylose, one should investigate mutations that destabilize the predominantly helical form of amylose in favor of more extended conformations, for example, by making substitutions at the O-2 sites.

4. Experimental

4.1. Force field

All the simulations and analyses were carried out using the GROMOS96 package[42,43] and the recently developed GROMOS force-field parameters for carbohydrates, which are summarized in Table 4.[44,45] To model the water molecules the simple point charge model (SPC)[46] was taken, one of the water models most widely used in biomolecular simulations.

4.2. System setup

The simulations are summarized in Table 1. The initial solute conformations of all the systems containing amylose fragments were, unless otherwise noted, the regular helical structure built from the data obtained by Imberty and Pérez.[3] It is characterized by the torsional angles of $\phi = \angle$O-5–C-1–O-4′–C-4′ $= 84°$ and $\psi = \angle$C-1–O-4′–C-4′–C-5′ $= -145°$. The simulations of amylose called SE and SEPERT started from a conformation with $\phi = 120°$ and $\psi = 60°$. The simulation called Maltose started with $\phi = 120°$ and $\psi = -120°$. All the simulations containing cellulose fragments (including cellobiose) started from an extended conformation with $\phi = -120°$ and $\psi = -120°$.

For each simulation the solute was placed at the center of a periodic truncated octahedral box. The minimum distance from any solute atom in the initial configuration to the square box walls was chosen to be at least 1.4, 1.9, or 2.0 nm (depending on the size and shape of the solute). The solvent molecules were introduced into the box by using a cubic periodic configuration of 216 pre-equilibrated water molecules. The resulting numbers of solvent molecules in the systems are specified in Table 1.

A steepest-descent energy minimization of the systems was performed to relax the solute–solvent contacts, while positionally restraining the solute atoms using a harmonic interaction with a force constant of 2.5×10^4 kJ mol^{-1} nm^{-2}. Next, steepest-descent energy minimization of the system without restraints was performed to eliminate any residual strain. The energy minimizations were terminated when the energy change per step became smaller than 0.1 kJ mol^{-1}.

4.3. Simulation protocol

The MD simulations started by taking initial velocities from a Maxwellian distribution at 100 K. Solvent and solute were independently, weakly coupled to a temperature bath with a relaxation time of 0.1 ps.[47] The systems were also isotropically, weakly coupled to a pressure bath at 1 atm with a relaxation time of 0.5 ps and an isothermal compressibility of 0.7513×10^{-3} (kJ mol^{-1} nm^{-3})$^{-1}$. Bond lengths were constrained using the SHAKE algorithm.[48] The time step for the leap-frog integration was 0.002 ps. For the nonbonded interactions, a triple-range method with cutoff radii of 0.8/1.4 nm was used. Short-range van der Waals and electrostatic interactions were evaluated every time step by using a charge-group pairlist. Medium-range van der Waals and electrostatic interactions, between pairs at a distance longer than 0.8 nm and shorter than 1.4 nm, were evaluated every fifth time step, at which point the pair list was updated, and kept constant between updates. Outside the longer cutoff radius a reaction-field approximation[49] was used with a relative dielectric permittivity of 78.5. The center of mass motion of the whole system was removed every 500 time steps. 200 ps of MD simulation with harmonic position restraining of the solute atoms were performed to further equilibrate the systems. The trajectory coordinates and energies were saved every 0.5 ps for analysis.

Table 4. Parameters of the GROMOS force field for carbohydrates[45] used in the present study

Atom			IAC	Partial charge (e)
C-1, C-2, C-3, C-4			12	0.232
C-5			12	0.376
C-6			13	0.232
O-1, O-4			3	−0.360
O-2, O-3, O-6			3	−0.642
O-5			3	−0.480
H-2, H-3, H-6			18	0.410
Me-2, Me-3, Me-6			14	0.180
Bond length			b_0 (nm)	K_b (10^6 kJ mol^{-1} nm^{-4})
C–O			0.1435	6.10
C–C			0.152	5.43
O–H			0.100	15.7
O–Me			0.1435	6.10
Bond angle			θ_0 (deg)	K_θ (kJ mol^{-1})
C–O–H			109.5	450
C–C–O			109.5	320
C–C–C			109.5	285
C–O–C			109.5	380
C–O–Me			109.5	380
Improper dihedral angle	Description		ξ_0 (deg)	K_ξ (kJ mol^{-1} deg^{-2})
C-1–O-5–O-4′–C-2	α-Linkage		35.26439	0.102
C-1–O-4′–O-5–C-2	β-Linkage		35.26439	0.102
C-5–O-5–C-6–C-4, C-2–O-2–C-3–C-1			35.26439	0.102
C-3–O-3–C-2–C-4, C-4–C-3–O-4–C-5			35.26439	0.102
Torsional angle	Description	cos(δ)	m	K_ϕ (kJ mol^{-1})
C-4′–O-4′–C-1–O-5	α-Linkage	−1.0	1	9.45
C-4′–O-4′–C-1–O-5	α-Linkage	1.0	3	3.65
C-4′–O-4′–C-1–O-5	β-Linkage	−1.0	1	3.41
C-4′–O-4′–C-1–O-5	β-Linkage	1.0	2[a]	4.69
O-4′–C-1–C-2–C-3		1.0	3	5.92
O-4′–C-1–C-2–C-3, O-5–C-1–C-2–C-3		1.0	2	0.418
O-4′–C-1–C-2–O-2, O-5–C-1–C-2–O-2		1.0	2	2.09
C-1–C-2–C-3–C-4, C-2–C-3–C-4–C-5, C-6–C-5–C-4–C-3		1.0	3	5.92
C-1–C-2–C-3–O-3, C-2–C-3–C-4–O-4, O-5–C-5–C-4–C-3		1.0	2	0.418
O-2–C-2–C-3–C-4, O-3–C-3–C-4–C-5, C-6–C-5–C-4–O-4		1.0	2	0.418
O-2–C-2–C-3–O-3, O-3–C-3–C-4–O-4, O-5–C-5–C-4–O-4		1.0	2	2.09
C-1–C-2–O-2–H-2, C-2–C-3–O-3–H-3, C-5–C-6–O-6–H-6		1.0	3	3.90
C-2–C-1–O-5–C-5, C-1–O-5–C-5–C-4		1.0	3	3.77
O-5–C-5–C-6–O-6		−1.0	1	9.35
O-5–C-5–C-6–O-6		1.0	3	9.50
C-1–C-2–O-2–Me-2, C-2–C-3–O-3–Me-3, C-5–C-6–O-6–Me-6		1.0	3	3.90

The atom names of the (united) atoms are defined in Figures 1 and 2. The methyl group, which is used to methylate O-2, O-3, and O-6 atoms is indicated as Me. The partial charges of atoms C-2, C-3, and C-6 are 0.180 e and those of atoms O-2, O-3, and O-6 are −0.360 e when the hydroxyl groups are methylated. The GROMOS96 integer atom code (IAC) defines the Lennard–Jones parameters of the corresponding atoms. The functional form of the force field is given in Refs. 42 and 43.

[a]This value differs from the value of 3 of the latest version of the GROMOS96 force field for carbohydrates.[45]

4.4. Single-step perturbation simulations

The single-step perturbation methodology[28,42] makes use of the fact that the free-energy perturbation formula for calculation the free-energy difference between two states a and b with Hamiltonian $H(\lambda)$ defined by $\lambda = \lambda_a$ and $\lambda = \lambda_b$

$$\Delta G_{ba} = G(b) - G(a) = -kT \ln \left\langle e^{-(H(\lambda_b) - H(\lambda_a))/kT} \right\rangle_{\lambda_a} \quad (1)$$

where the brackets represent an ensemble average over the configurations corresponding to the state $\lambda = \lambda_a$, requires no simulation in the state $\lambda = \lambda_b$ to calculate the free-energy difference. This means, in principle that a single simulation can be used to predict the relative free-energy differences between a native molecule (state a) and a great number of its mutants (states b, b′, b″, etc.). However, the reliability of the results is highly dependent on whether the configurations sampled in the state $\lambda = \lambda_a$ are representative for the ensembles of configurations of the collection of mutants (b, b′, b″, etc.). To ensure enough sampling, in the single-step perturbation technique a single nonphysical reference state (R) is

chosen that samples maximally the collection of mutant end states of interest. The single-step perturbation simulations (SHPERT, SEPERT, and CEPERT) were carried out for 5 ns under the same conditions as the simulations SH, SE, and CE described previously. In order to maximize the sampling at the methylation sites, all the hydroxyl groups in the amylose and cellulose fragments except for the two terminal ones were treated as soft-core interaction sites for the van der Waals and electrostatic interactions with the soft-core parameter values $\alpha_{LJ} = 1.51$ and $\alpha_C = 0.3\,\mathrm{nm}^2$.[50] The free-energy difference ΔG_{ba} can then be estimated from a single simulation of the reference state R using

$$\Delta G_{ba} = \Delta G_{bR} - \Delta G_{aR} \tag{2}$$

In this way, we are able to efficiently but approximately estimate the solvation free-energy differences for a huge number of mutants from a single simulation. Since the amylose and cellulose fragments studied here have nine glucopyranosyl units each with three-hydroxyl groups that can be methylated, we can obtain free-energy differences for $2^{27} - 1 = 134,217,727$ methylated derivatives of a nonaose. We only reported 31 of these (Table 3).

4.5. Analysis

According to their definition, generalized order parameters S^2 may be directly calculated from a simulation using the long-time tail of the second-order Legendre function of the reorientation correlation function of the C–H vector ($\vec{v}$):

$$S^2 = \lim_{t\to\infty} C_2(t) \tag{3}$$

where

$$C_2(t) = \langle P_2(\vec{v}(\tau)\cdot\vec{v}(\tau+t))\rangle_\tau \tag{4}$$

Here P_2 is the second-order Legendre polynomial, $P_2(x) = 1/2(3x^2 - 1)$. The angular brackets ($\langle\ \rangle$) represent the average over the ensemble (trajectory). The unit vectors $\vec{v}(\tau)$ and $\vec{v}(\tau + t)$ describe the orientation of the C–H vector at times τ and $\tau + t$ in relation to a fixed reference frame. To construct this frame, the translational and overall rotational motions were removed by a root-mean-square fitting of all the C-1, C-2, C-3, C-4, O-4, C-5, and O-5 atoms onto the starting conformation. In the GROMOS96 45A3 force field[44] aliphatic hydrogen atoms are not explicitly treated, but are part of united atoms. So all the C–H vectors were constructed according to the ideal tetrahedral carbon structure. In practice, expressions (3) and (4) are not very suitable to obtain accurate results, since the long-time tail of a correlation function is generally plagued by poor statistics. Therefore, the alternative formula[51,52]

$$S^2 = \frac{1}{2}\left[3\sum_{\alpha=1}^{3}\sum_{\beta=1}^{3}\langle v_\alpha(t)v_\beta(t)\rangle_t^2 - 1\right] \tag{5}$$

is used, which involves trajectory averages of the elements $v_\alpha v_\beta$ of the Cartesian tensor built as a direct product of the Cartesian components of the unit vector $\vec{v}(t)$, and yields, therefore, more accurate results. The average of S^2 is either taken over all configurations at 0.5 ps intervals of the whole simulation or by using an averaging window of 25 ps moving through the whole 2 ns simulation period.[39,53]

A conformational cluster analysis was performed on all the trajectories from the simulations using conformations at every 0.5 ps. Clustering was done as described in Ref. 54 by performing a rotational and translational atom-positional least-squares fit on every pair of conformations using atoms C-1, C-2, C-3, C-4, O-4, C-5, and O-5 and calculating the atom-positional root-mean-square deviation (RMSD) between two structures using these atoms. The similarity criteria used were an RMSD smaller or equal than 0.10, 0.15, and 0.21 nm for heptaose, nonaose (single helix), and nonaose (double helix), respectively. The cluster analysis was performed for the structures from the individual 5 ns simulation trajectories as well as for the trajectory of the unsubstituted nonaose merged with the trajectory of the various methylated derivatives. In the latter case conformations at every 1.0 ps were used.

As criterion for the occurrence of a hydrogen bond in a given structure a maximum distance of 0.25 nm between the hydrogen atom and the acceptor atom and a minimum donor–hydrogen–acceptor angle of 135° were used.

Acknowledgements

We would like to thank Dr. Roberto Lins for developing the new GROMOS force-field parameters for carbohydrates and Chris Oostenbrink for helpful discussion on free-energy calculations.

References

1. Buléon, A.; Colonna, P.; Planchot, V.; Ball, S. *Int. J. Biol. Macromol.* **1998**, *23*, 85–112.
2. Imberty, A.; Chanzy, H.; Pérez, S.; Buléon, A.; Tran, V. *J. Mol. Biol.* **1988**, *201*, 365–378.
3. Imberty, A.; Pérez, S. *Biopolymers* **1988**, *27*, 1205–1221.
4. Rappenecker, G.; Zugenmaier, P. *Carbohydr. Res.* **1981**, *89*, 11–19.
5. Godet, M. C.; Bizot, H.; Buléon, A. *Carbohydr. Polym.* **1995**, *27*, 47–52.
6. Saitô, H.; Yamada, J.; Yukumoto, T.; Yajima, H.; Endo, R. *Bull. Chem. Soc. Jpn.* **1991**, *64*, 3528–3537.
7. O'Sullivan, A. C. *Cellulose* **1997**, *4*, 173–207.
8. Zugenmaier, P. *Prog. Polym. Sci.* **2001**, *26*, 1341–1417.

9. Robyt, J. F. *Essentials of Carbohydrate Chemistry*; Springer: New York, 1998.
10. Woods, R. In *Rev. Comput. Chem.*; Lipowitz, K. B., Boyd, D. B., Eds.; VCH: New York, 1996; pp 129–165.
11. Imberty, A.; Pérez, S. *Chem. Rev.* **2000**, *100*, 4567–4588.
12. Sugiyama, H.; Hisamichi, K.; Usui, T.; Sakai, K.; Ishiyama, J. *J. Mol. Struct.* **2000**, *556*, 173–177.
13. Best, R. B.; Jackson, G. E.; Naidoo, K. J. *J. Phys. Chem. B* **2001**, *105*, 4742–4751.
14. Leeflang, B. R.; Vliegenthart, J. F. G.; Kroonbatenburg, L. M. J.; Vaneijck, B. P.; Kroon, J. *Carbohydr. Res.* **1992**, *230*, 41–61.
15. Glennon, T. M.; Zheng, Y. J.; Legrand, S. M.; Shutzberg, B. A.; Merz, K. M. *J. Comput. Chem.* **1994**, *15*, 1019–1040.
16. Ott, K. H.; Meyer, B. *Carbohydr. Res.* **1996**, *281*, 11–34.
17. Koehler, J.; Saenger, W.; van Gunsteren, W. F. *Eur. Biophys. J. Biophys. Lett.* **1987**, *15*, 197–210.
18. Koehler, J.; Saenger, W.; van Gunsteren, W. F. *Eur. Biophys. J. Biophys. Lett.* **1987**, *15*, 211–224.
19. Koehler, J.; Saenger, W.; van Gunsteren, W. F. *J. Biomol. Struct. Dyn.* **1988**, *6*, 181–198.
20. Koehler, J.; Saenger, W.; van Gunsteren, W. F. *Eur. Biophys. J. Biophys. Lett.* **1988**, *16*, 153–168.
21. Koehler, J.; Saenger, W.; van Gunsteren, W. F. *J. Mol. Biol.* **1988**, *203*, 241–250.
22. Varady, J.; Wu, X. W.; Wang, S. M. *J. Phys. Chem. B* **2002**, *106*, 4863–4872.
23. Bea, I.; Jaime, C.; Kollman, P. *Theor. Chem. Acc.* **2002**, *108*, 286–292.
24. Kirschner, K. N.; Woods, R. J. *Proc. Natl. Acad. Sci. U.S.A.* **2001**, *98*, 10541–10545.
25. Kony, D.; Damm, W.; Stoll, S.; van Gunsteren, W. F. *J. Comput. Chem.* **2002**, *23*, 1416–1429.
26. Trommsdorff, U.; Tomka, I. *Macromolecules* **1995**, *28*, 6128–6137.
27. Shimada, J.; Kaneko, H.; Takada, T.; Kitamura, S.; Kajiwara, K. *J. Phys. Chem. B* **2000**, *104*, 2136–2147.
28. Liu, H. Y.; Mark, A. E.; van Gunsteren, W. F. *J. Phys. Chem.* **1996**, *100*, 9485–9494.
29. Parfondry, A.; Cyr, N.; Perlin, A. S. *Carbohydr. Res.* **1977**, *59*, 299–309.
30. Pérez, S.; Taravel, F.; Vergelati, C. *Nouv. J. Chim.* **1985**, *9*, 561–564.
31. Shashkov, A. S.; Lipkind, G. M.; Kochetkov, N. K. *Carbohydr. Res.* **1986**, *147*, 175–182.
32. Cheetham, N. W. H.; Dasgupta, P.; Ball, G. E. *Carbohydr. Res.* **2003**, *338*, 955–962.
33. Rees, D. A. In *Outline Studies in Biology*; Ashworth, J., Ed.; Chapman and Hall Ltd: New York, 1977; pp 1–80.
34. Tvaroška, I.; Hricóvini, M.; Petráková, E. *Carbohydr. Res.* **1989**, *189*, 359–362.
35. Boelens, R.; Vuister, G. W.; Koning, T. M. G.; Kaptein, R. *J. Am. Chem. Soc.* **1989**, *111*, 8525–8526.
36. Yu, H. B.; Daura, X.; van Gunsteren, W. F. *Proteins* **2004**, *54*, 116–127.
37. Yu, H. B.; Ramseier, M.; Bürgi, R.; van Gunsteren, W. F. *ChemPhysChem*, **2004**, *5*, 633–641.
38. Lipari, G.; Szabo, A. *J. Am. Chem. Soc.* **1982**, *104*, 4546–4559.
39. Evenäs, J.; Forsén, S.; Malmendal, A.; Akke, M. *J. Mol. Biol.* **1999**, *289*, 603–617.
40. Peter, C.; Daura, X.; van Gunsteren, W. F. *J. Biomol. NMR* **2001**, *20*, 297–310.
41. Sugiyama, H.; Nitta, T.; Horii, M.; Motohashi, K.; Sakai, J.; Usui, T.; Hisamichi, K.; Ishiyama, J. *Carbohydr. Res.* **2000**, *325*, 177–182.
42. van Gunsteren, W. F.; Billeter, S. R.; Eising, A. A.; Hünenberger, P. H.; Krüger, P.; Mark, A. E.; Scott, W. R. P.; Tironi, I. G. Biomolecular Simulation: The GROMOS Manual and User Guide.; vdf Hochschulverlag, ETH Zürich: Switzerland, 1996.
43. Scott, W. R. P.; Hünenberger, P. H.; Tironi, I. G.; Mark, A. E.; Billeter, S. R.; Fennen, J.; Torda, A. E.; Huber, T.; Krüger, P.; van Gunsteren, W. F. *J. Phys. Chem. A* **1999**, *103*, 3596–3607.
44. Schuler, L. D.; Daura, X.; van Gunsteren, W. F. *J. Comput. Chem.* **2001**, *22*, 1205–1218.
45. Lins, R. D.; Hünenberger, P. H., in preparation.
46. Berendsen, H. J. C.; Postma, J. P. M.; van Gunsteren, W. F.; Hermans, J. In *Intermolecular forces*; Pullman, B., Ed.; Dordrecht: Reidel, 1981; pp 331–342.
47. Berendsen, H. J. C.; Postma, J. P. M.; van Gunsteren, W. F.; Di Nola, A.; Haak, J. R. *J. Chem. Phys.* **1984**, *81*, 3684–3690.
48. Ryckaert, J.-P.; Ciccotti, G.; Berendsen, H. J. C. *J. Comput. Phys.* **1977**, *23*, 327–341.
49. Tironi, I. G.; Sperb, R.; Smith, P. E.; van Gunsteren, W. F. *J. Chem. Phys.* **1995**, *102*, 5451–5459.
50. Schäfer, H.; van Gunsteren, W. F.; Mark, A. E. *J. Comput. Chem.* **1999**, *20*, 1604–1617.
51. Henry, E. R.; Szabo, A. *J. Chem. Phys.* **1985**, *82*, 4753–4761.
52. van Gunsteren, W. F.; Bakowies, D.; Damm, D.; Hansson, T.; Stocker, U.; Daura, X. In *Dynamics, Structure and Function of Biological Macromolecules*; Jardetzky, O., Finucane, M. D., Eds.; NATO ASI Series A; IOS: Amsterdam, 2001; Vol. 315, pp 1–26.
53. Stocker, U.; Spiegel, K.; van Gunsteren, W. F. *J. Biomol. NMR* **2000**, *18*, 1–12.
54. Daura, X.; van Gunsteren, W. F.; Mark, A. E. *Proteins* **1999**, *34*, 269–280.